

Single-cell profiling of breast cancer T cells reveals a tissue-resident memory subset associated with improved prognosis

Peter Savas^{1,2,13}, Balaji Virassamy^{1,13}, Chengzhong Ye^{3,4,5}, Agus Salim^{3,6}, Christopher P. Mintoff¹, Franco Caramia¹, Roberto Salgado^{1,7}, David J. Byrne⁸, Zhi L. Teo^{1,2}, Sathana Dushyanthen¹, Ann Byrne¹, Lironne Wein¹, Stephen J. Luen¹, Catherine Poliness⁹, Sophie S. Nightingale⁹, Anita S. Skandarajah^{9,10}, David E. Gyorki⁹, Chantel M. Thornton⁹, Paul A. Beavis^{1,2}, Stephen B. Fox^{10,2,8}, Kathleen Cunningham Foundation Consortium for Research into Familial Breast Cancer (kConFab), Phillip K. Darcy^{1,2}, Terence P. Speed^{3,11}, Laura K. Mackay^{10,12,14}, Paul J. Neeson^{1,2,14*} and Sherene Loi^{1,2,14*}

The quantity of tumor-infiltrating lymphocytes (TILs) in breast cancer (BC) is a robust prognostic factor for improved patient survival, particularly in triple-negative and HER2-overexpressing BC subtypes¹. Although T cells are the predominant TIL population², the relationship between quantitative and qualitative differences in T cell subpopulations and patient prognosis remains unknown. We performed single-cell RNA sequencing (scRNA-seq) of 6,311 T cells isolated from human BCs and show that significant heterogeneity exists in the infiltrating T cell population. We demonstrate that BCs with a high number of TILs contained CD8⁺ T cells with features of tissue-resident memory T (T_{RM}) cell differentiation and that these CD8⁺ T_{RM} cells expressed high levels of immune checkpoint molecules and effector proteins. A CD8⁺ T_{RM} gene signature developed from the scRNA-seq data was significantly associated with improved patient survival in early-stage triple-negative breast cancer (TNBC) and provided better prognostication than CD8 expression alone. Our data suggest that CD8⁺ T_{RM} cells contribute to BC immuno-surveillance and are the key targets of modulation by immune checkpoint inhibition. Further understanding of the development, maintenance and regulation of T_{RM} cells will be crucial for successful immunotherapeutic development in BC.

To explore both qualitative and quantitative aspects of T cells in BC TILs, a prospective cohort of patients ($n=123$; Supplementary Fig. 1 and Supplementary Table 1) with primary ($n=84$) or metastatic (nodal or distant, $n=45$) BCs were analyzed for their TIL content and T cell subsets using multiparameter flow cytometry (Fig. 1 and Supplementary Figs. 2–7). We observed that the overall per-

centage of TILs (CD45⁺) out of all live cells was significantly higher in primary (treatment-naive) than in metastatic tumor samples, and this did not change according to each BC subtype: TNBC, HER2-overexpressing (HER2⁺) and hormone receptor-positive (luminal) (Fig. 1a). A subset of BC samples, 20% of primary tumors and 46% of metastatic samples had <1% TIL content and hence could not be further analyzed. CD3⁺ T cells were the dominant TIL population in this BC cohort (Supplementary Fig. 5a); higher percentages of CD3⁺ TILs correlated with a significantly decreased CD4:CD8 ratio (Supplementary Fig. 5b). This observation is consistent with the notion that the presence of higher percentages of CD3⁺ T cells represents a more robust antigen-experienced, antitumor immune response and provides a biological rationale for previous observations that higher TIL levels in primary and metastatic BCs are associated with better outcomes¹. We next examined the frequency of naive and memory subsets of CD3⁺CD8⁺ and CD3⁺CD4⁺ T cells based on CD45RA and CCR7 expression (Supplementary Fig. 5d,e) and observed that the T effector memory (T_{EM}, CD45RA⁻CCR7⁻) followed by CD45RA⁺CCR7⁻ (T_{EMRA}) subsets were the most prevalent in primary BCs.

Immune checkpoint blockade inhibitors (CBI) have had modest efficacy to date in patients with BC^{3,4}. Nevertheless, higher response rates to pembrolizumab and atezolizumab have been reported to associate with the quantity of TILs in advanced TNBC⁵. To understand this observation, we explored which BC TIL subsets expressed immune checkpoints (Fig. 1b and Supplementary Figs. 5c and 6). Both CD3⁺CD4⁺ and CD3⁺CD8⁺ BC TILs expressed high levels of programmed cell death protein 1 (PD-1), but not T cell immunoglobulin and mucin domain-containing 3 (TIM-3)

¹Division of Research, Peter MacCallum Cancer Centre, University of Melbourne, Melbourne, Victoria, Australia. ²Sir Peter MacCallum Department of Oncology, University of Melbourne, Melbourne, Victoria, Australia. ³Bioinformatics Division, Walter & Eliza Hall Institute of Medical Research, Melbourne, Victoria, Australia. ⁴Department of Medical Biology, University of Melbourne, Melbourne, Victoria, Australia. ⁵School of Medicine, Tsinghua University, Beijing, China. ⁶Department of Mathematics and Statistics, La Trobe University, Melbourne, Victoria, Australia. ⁷Department of Pathology, GZA Ziekenhuizen, Antwerp, Belgium. ⁸Department of Pathology, Peter MacCallum Cancer Centre, Melbourne, Victoria, Australia. ⁹Division of Cancer Surgery, Peter MacCallum Cancer Centre, Melbourne, Victoria, Australia. ¹⁰Department of Surgery Royal Melbourne Hospital and Royal Womens' Hospital, University of Melbourne, Melbourne, Victoria, Australia. ¹¹Department of Mathematics and Statistics, University of Melbourne, Melbourne, Victoria, Australia. ¹²Department of Microbiology and Immunology, Peter Doherty Institute for Infection and Immunity, University of Melbourne, Melbourne, Victoria, Australia. ¹³These authors contributed equally: Peter Savas, Balaji Virassamy. ¹⁴These authors jointly directed this work: Laura K. Mackay, Paul J. Neeson, Sherene Loi. A full list of members and affiliations appears in the Supplementary Note. *e-mail: paul.neeson@petermac.org; sherene.loi@petermac.org

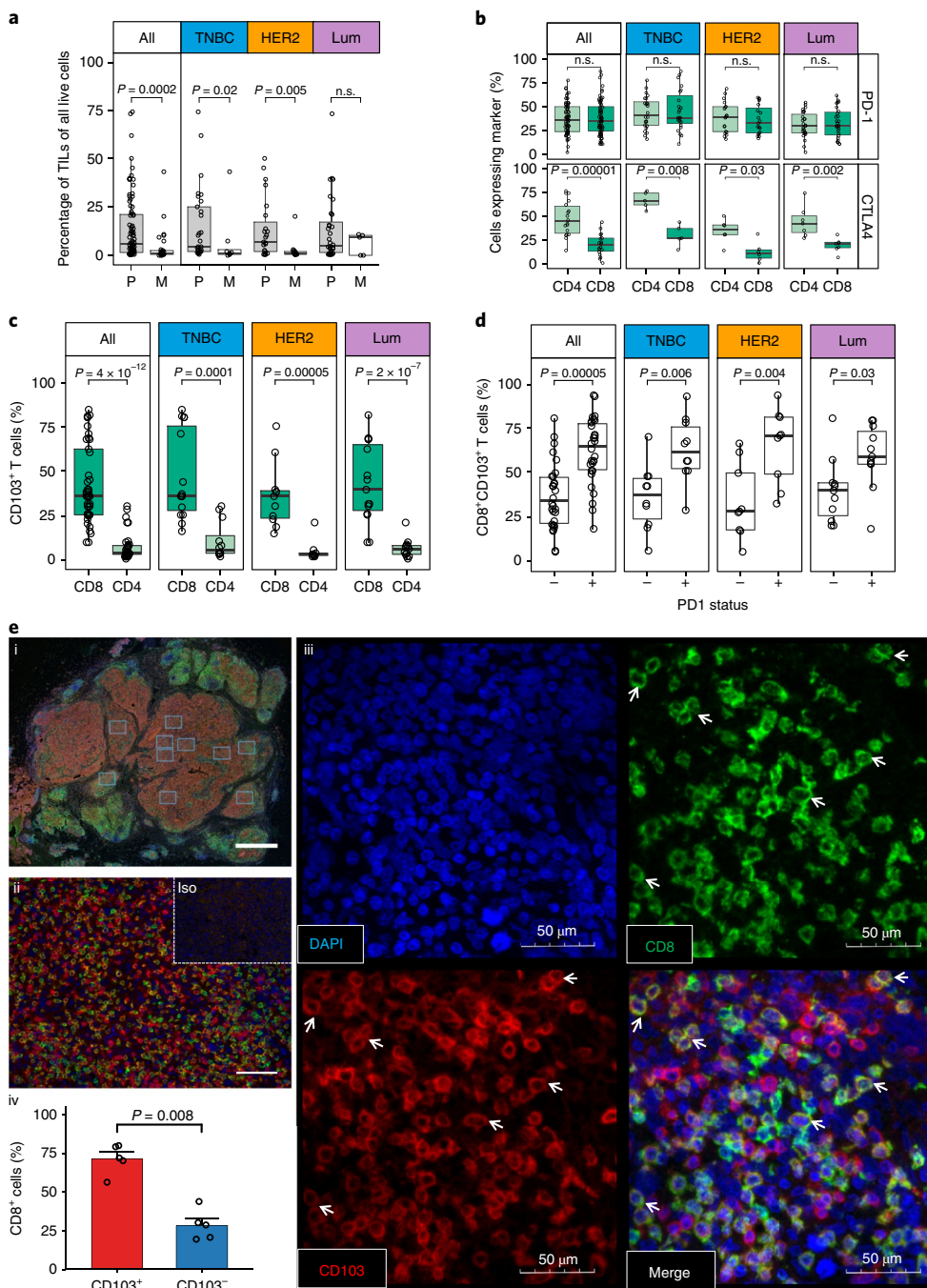


Fig. 1 | TILs in primary versus metastatic breast cancer, and CD8 populations expressing CD103. Patient TILs ($n=129$ independent cases) were harvested and underwent flow cytometry with a panel of T cell marker monoclonal antibodies. Viable cells were gated for MHC class I⁺CD45⁺ cells (TILs), T cells (CD3⁺) and CD3⁺CD4⁺ or CD3⁺CD8⁺ cells. **a**, The percentage of TILs out of all live cells in primary and metastatic tumors for the whole cohort (primary (P) $n=84$, metastatic (M) $n=26$, lymph node metastases excluded) and in tumors grouped according to breast cancer subtype: TNBC (primary $n=29$, metastatic $n=8$), HER2-positive (HER2, primary $n=23$, metastatic $n=13$) and hormone receptor-positive (Luminal (Lum), primary $n=32$, metastatic $n=5$). **b**, Prevalence of CD4 and CD8 subsets expressing the T cell checkpoints PD-1 (All $n=70$, TNBC $n=24$, HER2 $n=19$, Lum $n=27$) and CTLA4 (All $n=18$, TNBC $n=5$, HER2 $n=6$, Lum $n=7$). **c**, Expression of CD103 in CD3⁺CD8⁺ and CD3⁺CD4⁺ TILs (All CD8 $n=41$, CD4 $n=34$; TNBC CD8 $n=15$, TNBC CD4 $n=12$; HER2 CD8 $n=11$, HER2 CD4 $n=9$; Lum CD8 $n=15$, Lum CD4 $n=13$). **d**, PD-1 status in CD3⁺CD8⁺CD103⁺ TILs (All PD-1⁺ and PD-1⁻ $n=30$ and 30, TN PD-1⁺ and PD-1⁻ $n=10$ and 10, HER2 PD-1⁺ and PD-1⁻ $n=9$ and 9, Lum PD-1⁺ and PD-1⁻ $n=11$ and 11). **e**, Representative example of a primary TNBC stained by fluorescent multiplex immunohistochemistry showing coexpression of CD103 and CD8. Low-magnification image of whole tumor (**i**). Image at 20 \times magnification, with high numbers of CD8⁺ and CD103⁺ cells. Iso, isotype control (**ii**). Confocal images at 60 \times magnification of a single section stained for DAPI, CD8 and CD103, illustrating coexpression of CD8 and CD103 (small arrows) (**iii**). Scale bars: 2 mm (**i**), 100 μ m (**ii**), 50 μ m (**iii**). Quantification of CD103⁺ expression on CD8⁺ cells for $n=5$ independent cases, including representative case (**iv**). Bars show the mean percentage of CD8⁺ cells, and error bars are s.e.m.. Boxplots show the median (center bar), the third and first quartiles (upper and lower edge of box, respectively) and the largest and smallest value that is ≤ 1.5 times the interquartile range (limits of upper and lower whiskers, respectively). Data points, each representing one case, are shown by hollow circles. All statistical analyses were performed with the two-sided Wilcoxon rank-sum test without correction for multiple testing. n.s., nonsignificant.

or lymphocyte-activation gene-3 (LAG-3). Cytotoxic T lymphocyte-associated protein-4 (CTLA-4) was expressed at significantly higher levels by CD4⁺ versus CD8⁺ BC TILs. Regulatory T (T_{reg}) cells (CD4⁺FOXP3⁺) were present in generally low amounts in BC TILs. We did not observe any statistically significant difference in the proportion of T_{reg} cells between BC subtypes, though there was a trend to a higher proportion in TNBC (Supplementary Fig. 7a). We observed significantly higher coexpression of tumor necrosis factor receptor superfamily, member 4 (TNFRSF-4, also known as OX-40) and CTLA-4 on T_{reg} cells than on conventional CD4⁺FOXP3⁻ cells (Supplementary Fig. 7b). T_{reg} cells were either CTLA4^{hi}OX-40⁻PD-1⁻ or CTLA4^{lo}OX-40⁺PD-1⁻, whereas conventional CD4⁺FOXP3⁻ BC TILs were CTLA4^{hi}OX-40⁻PD-1⁺ or CTLA4^{lo}OX40⁺PD-1⁻ (Supplementary Fig. 7c).

The quantity of TILs in early-stage TNBC is strongly prognostic⁶; not surprisingly, TNBC is currently the chief BC subtype of interest for immunotherapeutic development. TNBC has the highest mutational burden of BC subtypes and likely the highest probability for generation of tumor neoantigens⁷. To interrogate the heterogeneity within the T cell infiltrate from human primary TNBCs in an unbiased manner, we performed 3' mRNA single-cell transcriptome analysis on 6,311 flow-sorted CD3⁺CD45⁺ T cells freshly isolated from two samples of human primary TNBC tumor (Fig. 2a). Mean reads per cell were 45,386 for the first sample and 218,263 for the second sample, with a median number of genes detected per cell of 833 and 1,347, respectively. Sequencing saturation was >90% for all samples, indicating comprehensive sampling of the available transcripts. After preprocessing, normalization and batch correction, unbiased clustering was performed. T cell clusters were visualized using t-distributed stochastic neighbor embedding (t-SNE) (Fig. 2b). We identified ten unique clusters based on their gene expression profiles (Fig. 2c). This included three distinct CD8A⁺ T cell clusters and four distinct CD4⁺ T cell clusters, including a T_{reg} (FOXP3⁺CTLA-4⁺) and a follicular CD4⁺CXCL13⁺ cell cluster⁸. These clusters were comparable across the two patients (Supplementary Fig. 8). Of interest, the T_{reg} cluster had strong expression of C-C motif chemokine receptor 8 (CCR8), which has only recently been reported to be specific to T_{reg} cells⁹. When focusing on the different CD8A⁺ clusters, we noted that one cluster had expression of molecules suggestive of a tissue-resident memory T (T_{RM}) cell phenotype. This CD8A⁺CD103⁺ T_{RM}-like cluster was highly distinct, with 400 genes at a false discovery rate (FDR) of <1% differentially expressed when compared with the other T cell clusters (Fig. 2d and Supplementary Table 2). This included high expression of the α_E chain (ITGAE, also known as CD103) of the integrin $\alpha_E\beta_7$ and significantly lower expression of SELL, KLRG1, KLF2, S1PR1 and S1PR5, akin to T_{RM} cells described in humans and mice^{10–13} (Fig. 2d and Supplementary Table 2). These molecules are hallmarks of T_{RM} differentiation and are necessary for retention of T_{RM} cells in tissue. Interestingly, in this cluster we also observed high expression of immune checkpoints, such as HAVCR2 (TIM3), PDCD1 (PD1), CTLA4, TIGIT and LAG3, and increased expression of granzyme B (GZMB) and perforin (PRF1) as compared with CD8A⁺CD103⁻ T cells (Fig. 2e and Supplementary Tables 2 and 3). We also analyzed CD8⁺ T cells using the Monocle 2 algorithm to establish a pseudo-temporal ordering reflective of cell lineage, inferred using the gene expression data¹⁴. As seen in Fig. 2f, the T_{RM}-like and T_{EM} cells were located at opposite ends of the pseudotime path, supporting the distinct gene expression profiles of these cells. The lack of branching in the path reflects the absence of distinct CD8 precursors and the terminally differentiated nature of CD8⁺ T cells in the microenvironment of primary tumors. Of interest, we also noticed an additional cluster of CD8A⁺CD103⁺ cells that displayed mitotic features, with high expression of genes associated with proliferation (Fig. 2c and Supplementary Fig. 9). This small cluster was located adjacent to the T_{RM} cluster in the pseudotime path (Fig. 2f) and is consistent with

a population of CD8⁺ T_{RM}-like cells actively undergoing cell division. Hence, we convincingly show using single-cell analysis that the CD8⁺ population is heterogeneous with distinct subsets. Of high interest for clinical development of immune agents was the CD8⁺ T_{RM}-like population, which expressed cytotoxic effector proteins as well as numerous immune checkpoints and retained the ability for active cell division in the immune microenvironment.

Nonrecirculating CD8⁺CD103⁺ T_{RM} cells have been shown to provide optimal immunity against infection¹⁵ and have recently been implicated in cancer immuno-surveillance^{16–18}. To further investigate the concept that CD8⁺ T cells with T_{RM} features are present in BCs with a high quantity of TILs, we used flow cytometry to evaluate CD103 expression on CD8⁺ T cells isolated from the human BCs used in Fig. 1a,b. We observed that the vast majority of CD8⁺ TILs expressed CD69 (Supplementary Fig. 3), likely reflective of the tumor microenvironment and not indicative of tissue residency in primary BCs¹⁹. In contrast, a variable subset of CD8⁺ T cells in BCs expressed CD103. These CD8⁺CD103⁺ T cells were present in significantly higher numbers than CD4⁺CD103⁺ T cells (Fig. 1c). We found a significant correlation between higher quantities of CD8⁺ T cells and these cells expressing CD103 (Supplementary Fig. 10a). The presence of CD8⁺ T cells also expressing CD103 was confirmed with multiplex and single-stain immunohistochemistry in primary TNBCs (Fig. 1e and Supplementary Fig. 11). Regarding immune checkpoint expression, a significantly higher percentage of CD8⁺CD103⁺ T cells also expressed PD-1 (Fig. 1d and Supplementary Fig. 10b). CD8⁺CD103⁺ T cells were more frequently positive for both CTLA-4 and PD-1 than CD8⁺CD103⁻ T cells (Supplementary Fig. 10c). Thus, our data strongly indicate that a CD8⁺CD103⁺ T cell population is enriched in BCs with a high number of TILs.

To confirm that human BC CD8⁺CD103⁺ T cells were similar to the T_{RM}-like cluster observed in the single-cell data, we performed bulk RNA-seq on FACS-sorted CD8⁺CD103⁺ and CD8⁺CD103⁻ T cells using fresh tumor samples from another three patients (two primary and one TNBC liver metastasis, Fig. 2a). We identified 534 significantly differentially expressed genes at FDR < 5% (Fig. 3a and Supplementary Table 4). In the CD8⁺CD103⁺ population, we again identified significantly decreased expression of tissue egress genes S1PR1 and KLF2 and significantly higher levels of immune checkpoints including PD1 and CTLA4. Hence, we confirmed that the CD8⁺CD103⁺ population is functionally and phenotypically different from the CD8⁺CD103⁻ subset in independent BC samples. The gene signature derived from bulk RNA-seq of CD8⁺CD103⁺ T cells was remarkably similar to our signature derived from the unbiased single-cell interrogation (Fig. 3a,b), as further supported using gene set enrichment analyses (Fig. 3c). Taken together, our data indicate that BC CD8⁺CD103⁺ T cells show features consistent with T_{RM} differentiation and establish that in BCs with a high number of TILs, high quantities of CD8⁺CD103⁺ T_{RM}-like cells are present, which appear to be a distinct subset^{13,15}.

To explore the functional characteristics of BC CD8⁺CD103⁺ T cells, we performed in vitro functional assays in which TILs were cocultured with autologous BC cells in the presence or absence of T cell receptor (TCR) stimulation. CD8⁺CD103⁺ T cells expressed significantly more granzyme B than CD8⁺CD103⁻ T cells (Fig. 3d). Furthermore, independent of CD3/CD28 stimulation, TILs from human TNBC samples secreted granzyme B and RANTES (CCL5) into the culture supernatant, whereas interferon- γ (IFN- γ) secretion required CD3/CD28 stimulation (Supplementary Fig. 10d). These data support the cytotoxic ability and proinflammatory potential of CD8⁺CD103⁺ T cells derived from human TNBCs.

Using the bulk RNA-seq from sorted CD8⁺CD103⁺ and CD8⁺CD103⁻ T cells from three samples (Fig. 3a–c), TCR- β sequences were extracted to infer T cell clonality. This analysis established that TCR clonotypes representing clonal T cell populations

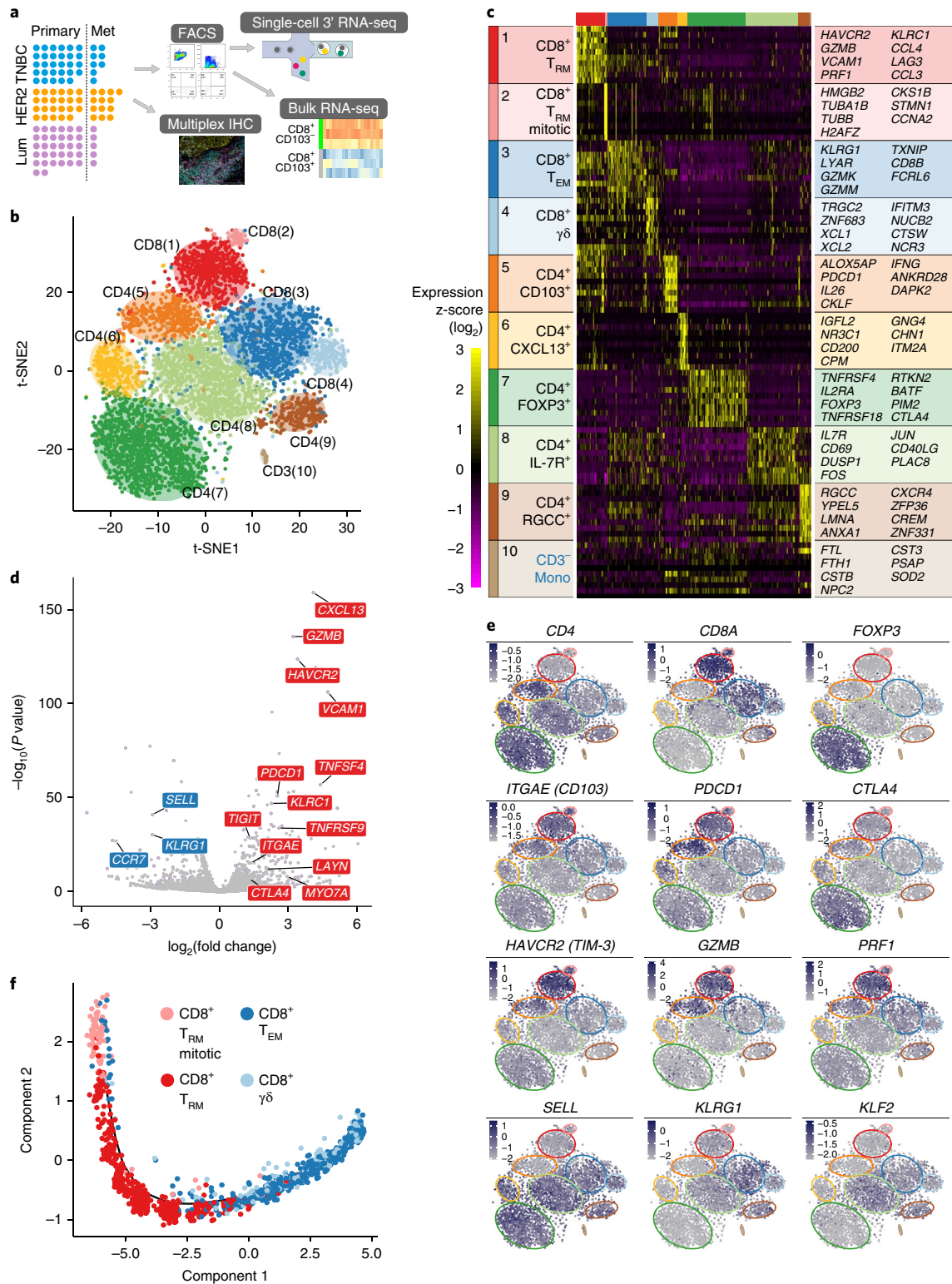


Fig. 2 | Single-cell RNA-seq of 6,311 purified CD3⁺ single T cells from human primary TNBCs. **a**, Workflow of both single-cell and bulk RNA-seq of human isolated T cells. **b**, t-SNE plot with clusters demarcated by colors demonstrating ten distinct clusters based on gene expression differences for 5,759 cells passing quality control. The numbers in parentheses correspond to the clusters listed in **c**. **c**, Heat map from single-cell analysis via expression recovery (SAVER) imputed data with cells grouped into clusters (indicated by colored bars at the top). The top ten genes differentially expressed for each cluster are shown on the y axis, and key genes are also shown for each cluster. **d**, Volcano plot showing key differentially expressed genes between CD8⁺ TRM-like ($n=685$ cells across both cases) and TEM-like clusters ($n=953$ cells across both cases). P values were derived using DECENT (see Methods), which employs a likelihood-ratio test. Unadjusted P values are shown. The full list of differentially expressed genes and associated statistics is in Supplementary Table 2. T_{RM} genes are shown in red, and T_{EM} genes are shown in blue. **e**, Feature plots demonstrating expression of key genes in the 5,759 cells. Color scale represents SAVER imputed gene expression value (\log_{10} scale) for each cell for a given gene. **f**, 2-D representation of $n=2,005$ cells in CD8⁺ clusters (indicated with colored circles) in single-cell data using the Monocle 2 algorithm.

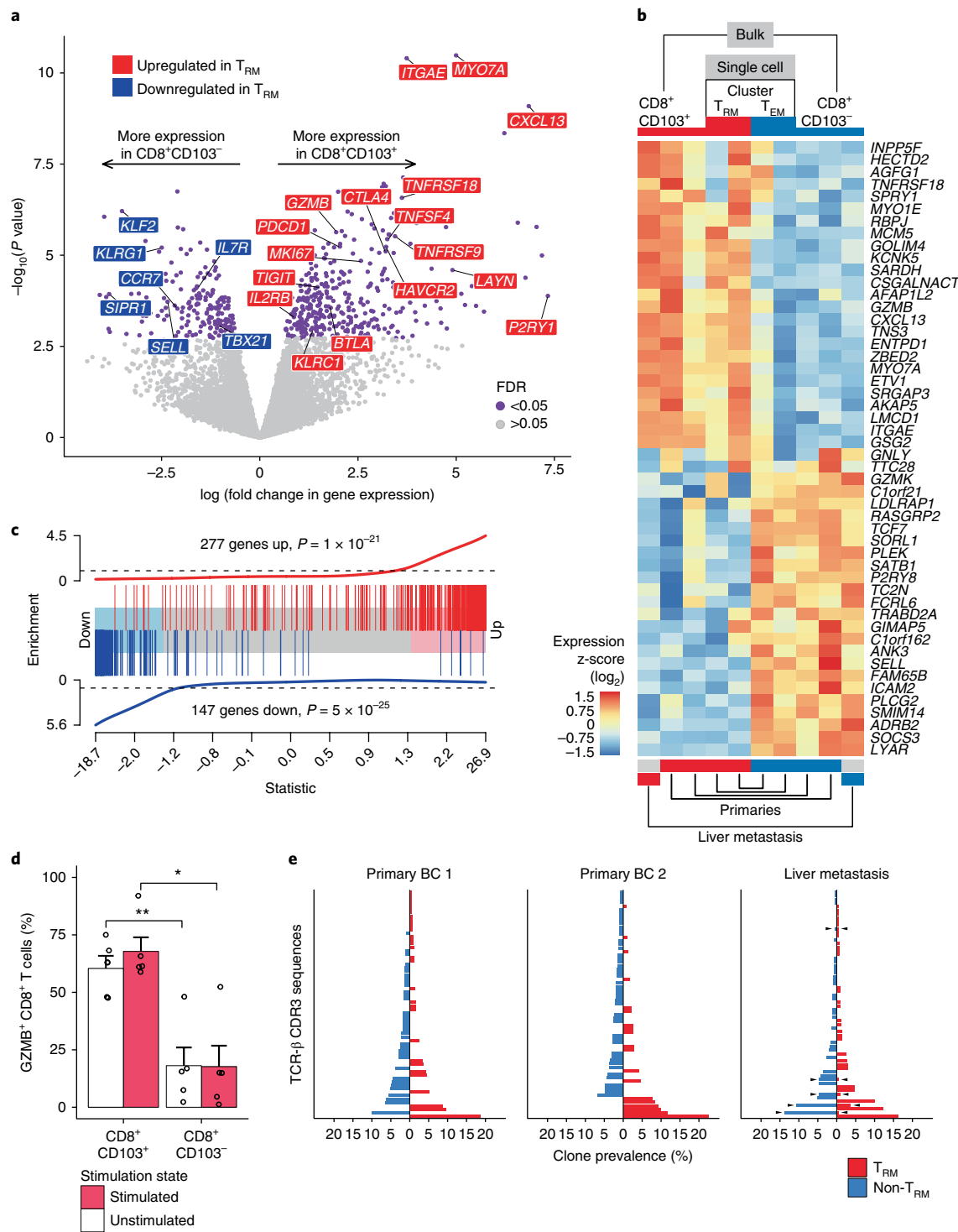


Fig. 3 | Characterization of $CD8^+CD103^+$ T cells using flow cytometry, bulk RNA-seq, functional studies and TCR repertoire. **a**, Volcano plot showing significantly differentiated genes according to $CD103$ expression in flow-sorted $CD8^+$ T cells from $n=3$ independent cases (two primary tumors and one liver metastasis). P values on the y axis were derived from empirical Bayes moderated t -statistics implemented by limma (see Methods). Unadjusted P values are shown. **b**, Heat map comparing gene signatures derived from bulk RNA-seq ($CD103$ positive versus negative) and T_{RM} cluster versus other T cells derived from the single-cell RNA-seq data. **c**, Using gene sets derived from genes differentially expressed between $CD103^+$ and $CD103^-$ $CD8^+$ T cells in bulk RNA-seq, barcode plot shows significant enrichment of bulk $CD8^+CD103^+$ 'UP' genes in the single-cell T_{RM} cluster and bulk $CD103^-$ 'UP' genes in the single-cell T_{EM} clusters (preranked competitive gene set test from limma). Statistic on the x axis is the gene wise z-score statistic from DECENT, and vertical bars represent statistic for each gene in the gene set. **d**, Granzyme B (GZMB) expression in $CD8^+CD103^+$ T cells as determined from in vitro functional data from $n=5$ patients with TNBC. Bars show the mean value, and error bars represent s.e.m.. Statistical analysis was performed with the two-sided Wilcoxon rank-sum test. **e**, Comparison of clonotypes between $CD8^+CD103^+$ T cells versus $CD8^+CD103^-$ T cells in primary tumors and liver metastasis. The primary tumors show no overlap between TCR repertoires. Overlapping clones are marked with arrowheads for the liver metastasis. Clonotypes with prevalence $<0.5\%$ were excluded for clarity.

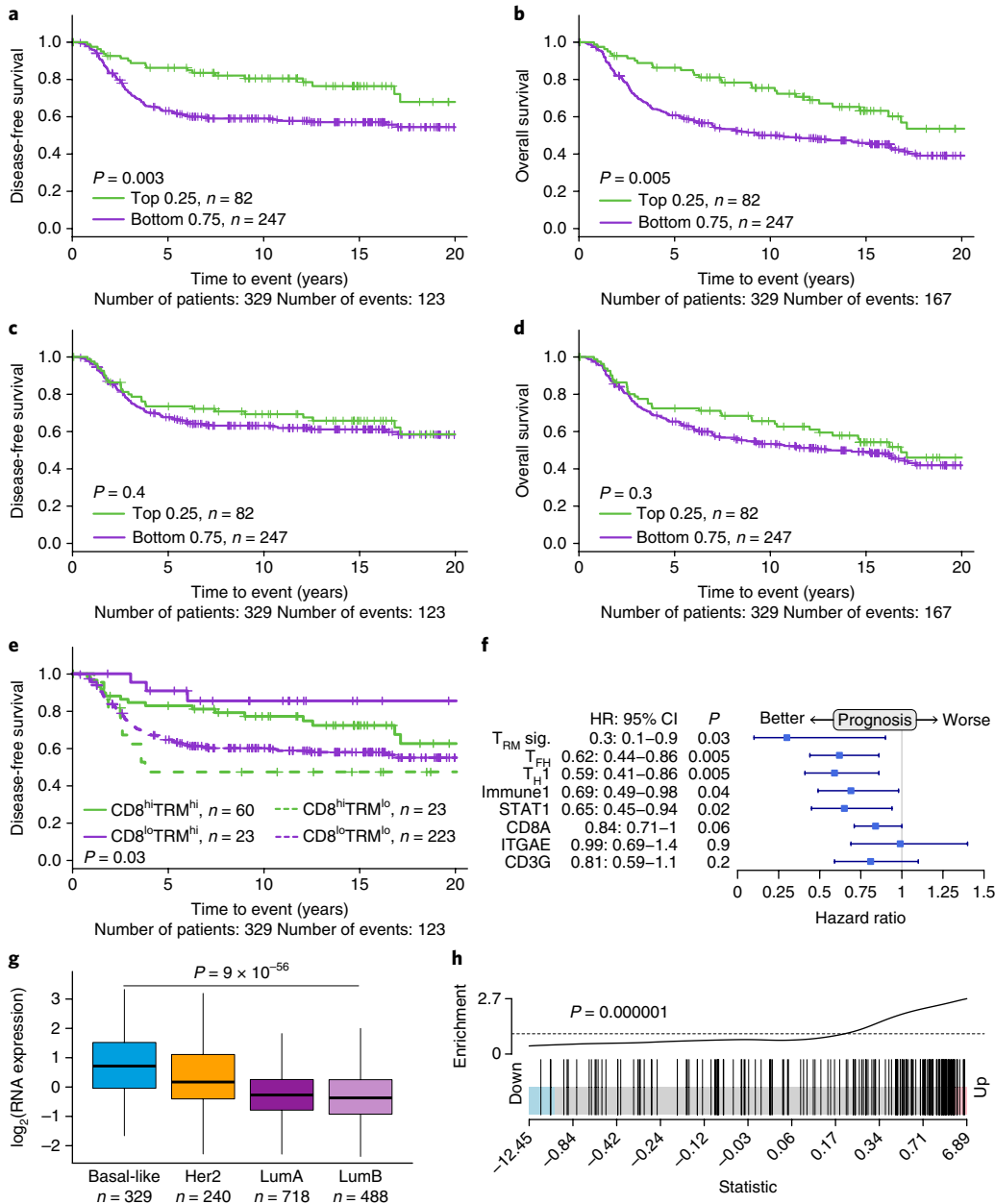


Fig. 4 | Superior prognostic abilities of the T_{RM} CD8⁺ gene signature derived from single-cell data in human early-stage TNBCs. **a,b**, Kaplan-Meier survival curves for disease-free survival (**a**) and overall survival (**b**) from $n=329$ primary basal-like/TNBCs showing significant prognostic separation according to T_{RM} gene signature derived from single-cell data. **c,d**, Disease-free (**c**) and overall (**d**) survival using CD8A expression to stratify cases. **e**, Disease-free survival for cases further stratified according to CD8 T_{RM} signature expression within CD8A expression strata. Log-rank P values are shown. **f**, Prognostic effect of T_{RM} signature compared to other T cell signatures (indicated on the y axis; see Methods) as well as single gene expression of CD3, CD8 and CD103 as continuous variables in 329 basal-like/TNBC primary breast cancers. Forest plots show HRs (blue squares) and confidence intervals (horizontal ranges) derived from Cox regression survival analyses for disease-free survival in multivariable analyses adjusted for age, nodal status, grade and tumor size. **g**, Boxplot showing relative enrichment of the T_{RM} gene signature in TNBC compared with other BC subtypes ($n=1,775$ cases). Statistical analysis was performed with the Kruskal-Wallis rank-sum test. Results were derived from the publicly available METABRIC consortium dataset. BC subtypes are taken from the published data. Boxplots show the median (center bar), the third and first quartiles (upper and lower edge of box, respectively) and the largest and smallest value that is ≤ 1.5 times the interquartile range (limits of upper and lower whiskers, respectively). **h**, T_{RM} signature enrichment in baseline tumor samples from responders ($n=9$) compared with nonresponders ($n=36$) to checkpoint blockade in patients with melanoma (limma ‘roast’ gene set test). Statistic on x axis is the gene wise moderated t-statistic computed by limma, and vertical bars represent t-statistic for each gene in the gene set.

were present in both T cell subsets. T_{RM} had numerically higher TCR clonality (mean T_{RM} clonality = 0.2, mean T_{EM} clonality = 0.11), and these clonalities were comparable to prior studies in metastatic melanoma^{20,21}. Of high interest, although we observed no common TCR clones with prevalence $>0.5\%$ between these populations in the pri-

mary breast tumors, the liver metastasis sample showed some overlap (Fig. 3e). These nonoverlapping TCR repertoires between T_{RM} and T_{EM} in the primary tumors suggest that the CD8⁺CD103⁺ T_{RM}-like cells have differing antigen specificity to T_{EM}. To further understand this phenomenon, we evaluated whether CD8⁺CD103⁺ T cells were

present in eight normal breast tissue specimens derived from prophylactic mastectomies. Although the proportion of lymphocytes in normal breast tissue is less than that of primary tumors (Supplementary Fig. 12a), CD8⁺CD103⁺ T cells make up a substantial proportion of the CD8⁺ T cells that are present (Supplementary Figs. 12 and 13b). Taken together, these data indicate that T_{RM} cells exhibit clonal expansion, which is typically associated with antigen recognition, and that their antigen specificity may arise from the differing microenvironment experienced during residence in normal, preneoplastic and early neoplastic breast tissue.

As our data suggest that the CD8⁺CD103⁺ T_{RM} cell subset is a highly prevalent effector population in the microenvironment of primary TNBCs, we predicted that the single-cell-derived gene signature from the T_{RM}-like cluster would provide important prognostic information. Using available gene expression data from the 'METABRIC' consortium, we found that the T_{RM} signature was significantly associated with improved relapse-free and overall survival in 329 primary TNBCs after standard chemotherapy (Fig. 4). Furthermore, we show that the T_{RM} signature can discriminate between patients with high CD8 expression who have a good or poor prognosis (Fig. 4e and Supplementary Fig. 14). We found that the T_{RM} signature was significantly associated with better prognosis, and the hazard ratios (HRs) observed were stronger than any of CD8, CD3 or CD103 single gene expression, as well as a published gene signatures representing T helper 1 (T_{H1}), T follicular helper (T_{FH}) and STAT1 processes^{8,22,23}. This suggests that the T_{RM} signature has a superior ability to discriminate prognostic groups in both univariable (Supplementary Fig. 14) and multivariable analyses (Fig. 4f). As expected, there was higher expression of the T_{RM} signature in TNBC than in the other BC subtypes (Fig. 4g). These data suggest that CD8⁺ T_{RM} cells may be the key mediator of the improved clinical outcomes observed in human BCs with a high quantity of TILs^{24–28}.

In conclusion, although CD8⁺ T cells are associated with good prognosis in BC^{29,30}, our work has demonstrated the importance of qualitative differences in BC CD8⁺ T cells subsets. We revealed these differences by using scRNA-seq of over 6,000 single T cells, which demonstrated that a large proportion of CD8⁺ T cells displayed a T_{RM} phenotype that was distinct from T_{EM}-like cells. We confirmed a significant association between the T_{RM} gene signature and improved survival from TNBC, the most aggressive BC subtype. Hence, both qualitative and quantitative differences in the T cell infiltrate influence survival of patients with BC.

Primary BC TIL numbers were significantly higher than those in metastatic biopsies, suggesting that relapsed BC is poorly immunogenic or immune hostile (Fig. 1a), a substantial challenge for the future refinement of checkpoint inhibition in this setting^{3,4}. Importantly, our data suggest that with their cytotoxic potential, strong expression of therapeutically tractable T cell checkpoints and evident capacity for cell proliferation, T_{RM} cells may be the key targets for immunotherapeutic modulation in patients with BC. The direct or indirect mechanisms whereby this would occur *in vivo* are unclear; the T_{RM} cells may respond to checkpoint inhibition by direct cytotoxicity or release of proinflammatory cytokines and chemokines that create a permissive immune microenvironment. In support of this, we evaluated a publicly available gene expression dataset of 68 melanoma samples from 45 patients treated with immune checkpoint blockade²⁰ and found a significant enrichment of the T_{RM} signature in responders at baseline (Fig. 4h) as well as significant upregulation of these genes in biopsies taken during treatment with the anti-PD-1 agent nivolumab as compared to baseline (Supplementary Fig. 15).

In summary, the BC T cell infiltrate quantity and quality, including the presence of the T_{RM} cell subset, are key to improved therapeutic and prognostic outcomes, particularly for patients with TNBC. Our study highlights the potential of single-cell genomics to increase our understanding of the tumor microenvironment and

potentially identify new immunotherapy targets. This data also provides a unique resource of transcriptome data from BC-infiltrating T cells that can be interrogated with a web-based tool (see URLs) by the wider research community. This information will be invaluable for understanding the many potential targets for immunotherapy approaches currently available.

URLs

BC-infiltrating T cells single-cell transcriptome data; <https://www.tilsinbreastcancer.org/researcher-resources>.

Methods

Methods, including statements of data availability and any associated accession codes and references, are available at <https://doi.org/10.1038/s41591-018-0045-3>.

Received: 28 November 2017; Accepted: 25 April 2018;

Published online: 25 June 2018

References

1. Savas, P. et al. Clinical relevance of host immunity in breast cancer: from TILs to the clinic. *Nat. Rev. Clin. Oncol.* **13**, 228–241 (2016).
2. Ruffell, B. et al. Leukocyte composition of human breast cancer. *Proc. Natl Acad. Sci. USA* **109**, 2796–2801 (2012).
3. Adams, S. et al. Phase 2 study of pembrolizumab (pembro) monotherapy for previously treated metastatic triple-negative breast cancer (mTNBC): KEYNOTE-086 cohort A. *J. Clin. Oncol.* **35** no. 15_suppl, 1008 (2017).
4. Schmid, P. et al. Atezolizumab in metastatic TNBC (mTNBC): long-term clinical outcomes and biomarker analyses. *Cancer Res.* **77**, 2986 (2017).
5. Loi, S. et al. Relationship between tumor infiltrating lymphocyte (TIL) levels and response to pembrolizumab (pembro) in metastatic triple-negative breast cancer (mTNBC): results from KEYNOTE-086. *Ann. Oncol.* **28**, LBA13 (2017).
6. Loi, S. et al. Pooled individual patient data analysis of stromal tumor infiltrating lymphocytes in primary triple negative breast cancer treated with anthracycline-based chemotherapy. *Cancer Res.* **76**, abstr. S1–03 (2015).
7. Nolan, E. et al. Combined immune checkpoint blockade as a therapeutic strategy for BRCA1-mutated breast cancer. *Sci. Transl. Med.* **9**, eaal4922 (2017).
8. Gu-Trantien, C. et al. CD4⁺ follicular helper T cell infiltration predicts breast cancer survival. *J. Clin. Invest.* **123**, 2873–2892 (2013).
9. Plitas, G. et al. Regulatory T cells exhibit distinct features in human breast cancer. *Immunity* **45**, 1122–1134 (2016).
10. Hombrink, P. et al. Programs for the persistence, vigilance and control of human CD8⁺ lung-resident memory T cells. *Nat. Immunol.* **17**, 1467–1478 (2016).
11. Kumar, B. V. et al. Human tissue-resident memory t cells are defined by core transcriptional and functional signatures in lymphoid and mucosal sites. *Cell Reports* **20**, 2921–2934 (2017).
12. Mackay, L. K. et al. The developmental pathway for CD103(+)/CD8⁺ tissue-resident memory T cells of skin. *Nat. Immunol.* **14**, 1294–1301 (2016).
13. Schenkel, J. M. & Masopust, D. Tissue-resident memory T cells. *Immunity* **41**, 886–897 (2014).
14. Trapnell, C. et al. The dynamics and regulators of cell fate decisions are revealed by pseudotemporal ordering of single cells. *Nat. Biotechnol.* **32**, 381–386 (2014).
15. Mueller, S. N. & Mackay, L. K. Tissue-resident memory T cells: local specialists in immune defence. *Nat. Rev. Immunol.* **16**, 79–89 (2016).
16. Malik, B. T. et al. Resident memory T cells in the skin mediate durable immunity to melanoma. *Sci. Immunol.* **2**, eaam6346 (2017).
17. Nizard, M. et al. Induction of resident memory T cells enhances the efficacy of cancer vaccine. *Nat. Commun.* **8**, 15221 (2017).
18. Ganeshan, A. P. et al. Tissue-resident memory features are linked to the magnitude of cytotoxic T cell responses in human lung cancer. *Nat. Immunol.* **18**, 940–950 (2017).
19. Thompson, E. D., Enriquez, H. L., Fu, Y. X. & Engelhard, V. H. Tumor masses support naive T cell infiltration, activation, and differentiation into effectors. *J. Exp. Med.* **207**, 1791–1804 (2010).
20. Riaz, N. et al. Tumor and microenvironment evolution during immunotherapy with nivolumab. *Cell* **171**, 934–949.e915 (2017).
21. Tumeh, P. C. et al. PD-1 blockade induces responses by inhibiting adaptive immune resistance. *Nature* **515**, 568–571 (2014).
22. Desmedt, C. et al. Biological processes associated with breast cancer clinical outcome depend on the molecular subtypes. *Clinical Cancer Res.* **14**, 5158–5165 (2008).

23. Teschendorff, A. E., Miremadi, A., Pinder, S. E., Ellis, I. O. & Caldas, C. An immune response gene expression module identifies a good prognosis subtype in estrogen receptor negative breast cancer. *Genome Biol.* **8**, R157 (2007).
24. Denkert, C. et al. Tumor-associated lymphocytes as an independent predictor of response to neoadjuvant chemotherapy in breast cancer. *J. Clin. Oncol.* **28**, 105–113 (2010).
25. Loi, S. et al. Tumor infiltrating lymphocytes (TILs) indicate trastuzumab benefit in early-stage HER2-positive breast cancer (HER2+ BC). *Cancer Res.* **73**, abstr. S1–05 (2013).
26. Loi, S. et al. Tumor infiltrating lymphocytes are prognostic in triple negative breast cancer and predictive for trastuzumab benefit in early breast cancer: results from the FinHER trial. *Ann. Oncol.* **25**, 1544–1550 (2014).
27. Luen, S. J. et al. Tumour-infiltrating lymphocytes in advanced HER2-positive breast cancer treated with pertuzumab or placebo in addition to trastuzumab and docetaxel: a retrospective analysis of the CLEOPATRA study. *Lancet Oncol.* **18**, 52–62 (2017).
28. Salgado, R. et al. Tumor-infiltrating lymphocytes and associations with pathological complete response and event-free survival in HER2-positive early-stage breast cancer treated with lapatinib and trastuzumab: a secondary analysis of the NeoALTTO trial. *JAMA Oncol.* **1**, 448–454 (2015).
29. Ali, H. R. et al. Association between CD8⁺ T-cell infiltration and breast cancer survival in 12,439 patients. *Ann. Oncol.* **25**, 1536–1543 (2014).
30. DeNardo, D. G. & Coussens, L. M. Inflammation and breast cancer. Balancing immune response: crosstalk between adaptive and innate immune cells during breast cancer progression. *BCR* **9**, 212 (2007).

Acknowledgements

We wish to thank H. Thorne, E. Niedermayr, all the kConFab research nurses and staff, the heads and staff of the Family Cancer Clinics and the Clinical Follow Up Study (which has received funding from the National Health and Medical Research Council of Australia (NHMRC), the National Breast Cancer Foundation (NBCF), Cancer Australia and the National Institute of Health (United States) for their contributions to this research, and the many families who contribute to kConFab. We wish to thank the FACS core facility staff R. Rossi, V. Milovac and S. Curcio, and T. Tan and P. Petrone for additional FACS assistance. We also thank S. Ellis for assistance with confocal imaging, G. M. Arnau for facilitating RNA-seq, and the Anatomical Pathology staff at the Peter MacCallum Cancer Centre. Special thanks also to J. Jabbari and the Australian Genome Research Facility for making the single-cell sequencing possible.

This study was funded by the Breast Cancer Research Foundation (BCRF), NY. S.L. is supported by the Cancer Council Victoria John Colebatch Fellowship and the National Breast Cancer Foundation. P.S. is supported by the NHMRC and the NBCF (Post Graduate Scholarship 1094388), the Cancer Therapeutics CRC and the Peter Mac Foundation. Z.L.T. is supported by the NHMRC (Early Career Fellowship 1106967). D.G. is supported by the Peter Mac Foundation. P.A.B. is supported by the NHMRC (Early

Career Fellowship 17-005). S.J.L is supported by the University of Melbourne. S.B.F. is supported by the NHMRC (Practitioner Fellowship 1079329). kConFab is supported by a grant from NBCF, and previously NHMRC, the Queensland Cancer Fund, the Cancer Councils of New South Wales, Victoria, Tasmania and South Australia, and the Cancer Foundation of Western Australia. P.K.D is supported by the NHMRC (Senior Research Fellowship 1136680 and Program Grant 1132373). T.S. is supported by the NHMRC (Program Grant 1054618). P.J.N. is supported by the NHMRC (Program Grant 1132373).

Author contributions

P.S. conceived and designed the study, provided and collected study materials and samples and patient data, performed experiments, analyzed data and wrote the manuscript. B.V. designed the study, provided and collected study materials and samples and patient data, performed experiments, analyzed data and wrote the manuscript. C.Y. developed analysis methods and software, analyzed data and wrote the manuscript. A.S. developed analysis methods and software, analyzed single-cell sequencing data and wrote the manuscript. C.P.M performed experiments, analyzed data and wrote the manuscript. F.C. analyzed data and wrote the manuscript. R.S. analyzed data and wrote the manuscript. D.J.B performed experiments and wrote the manuscript. Z.L.T. provided and collected study materials and samples, analyzed data and wrote the manuscript. S.D. performed experiments, analyzed data and wrote the manuscript. A.B. performed experiments, analyzed data and wrote the manuscript. L.W. provided and collected study materials and samples and patient data and wrote the manuscript. S.J.L. provided and collected study materials and samples and patient data and wrote the manuscript. C.P. provided and collected study materials and samples and patient data. S.S.N. provided and collected study materials and samples and patient data. A.S.S. provided and collected study materials and samples and patient data. D.E.G. provided and collected study materials and samples and patient data. C.M.T. provided and collected study materials and samples and patient data. P.A.B. analyzed data and wrote the manuscript. S.B.F provided and collected study materials and samples and patient data, analyzed data and wrote the manuscript. kConFab provided and collected study materials and samples. P.K.D. designed the study, analyzed data and wrote the manuscript. T.P.S. developed analysis methods and software, designed the study and wrote the manuscript. L.K.M. designed the study and wrote the manuscript. P.J.N. designed the study and wrote the manuscript. S.L. conceived and designed the study, provided and collected study materials and samples and patient data and wrote the manuscript.

Competing interests

The authors declare no competing interests.

Additional information

Supplementary information is available for this paper at <https://doi.org/10.1038/s41591-018-0078-7>.

Reprints and permissions information is available at www.nature.com/reprints.

Methods

Patient samples. This project was approved by the Human Research Ethics Committee of the Peter MacCallum Cancer Centre (project approval number 'SEGMENT' 13/123, Kathleen Cunningham Foundation Consortium for Research into Familial Breast Cancer (kConFab) project approval numbers 129 and 150). All participating patients provided written informed consent.

Reagents and antibodies. Antibodies used in this study included BV510-conjugated CD45 (CD45-BV510), CD127-BV421, CD3-APCH7, CD103-BV421, CD8-BV605, OX-40-PECy7, PD-1-BV785, CCR7-BV711, CD3-BV711, CD4-BV650, CD69-PerCP-Cy5.5, CTLA4-APC, Zombie red PETex-Red (Biologics, San Diego, CA); HLA-A,B,C-PECy5, CD45-FITC, CD8-PE, CD45RA-FITC, GZMB-PE, TNF- α -APC, IFN- γ -FITC (BD Biosciences, San Diego, CA) TIM-3 PerCP-EF710, and FOXP3-PE (e-Bioscience, San Diego, CA); LAG3-APC (R&D systems, Minneapolis, MN). The Nature Research Reporting Summary details all antibodies used (See Supplementary Information).

Isolation of TILs from breast cancer biopsies and healthy breast tissue.

Following tumor excision or biopsy, a representative tumor fragment that was fresh and sterile was transferred to the laboratory for study. All surrounding macroscopic tissue, including any obvious tumor capsule, was removed from the tumor. Tumor tissue was divided into segments and either placed in neutral buffered formalin for processing to formalin-fixed paraffin-embedded (FFPE) blocks, or a single-cell suspension was created using a modified published protocol³¹. Briefly, tumor was initially divided into segments and then finely diced into RPMI1640 containing 20% FBS, 1 mg/ml collagenase type 4 (Worthington Biochemical, Lakewood, NJ), 30 U/ml DNase (Roche diagnostics, Indianapolis, IN, USA), 10 μ g/ml gentamicin (Life Technologies, Waltham, MA, USA) and was incubated for 30 min at 37°C on a rocker. Digested tumor pieces were teased through a 70- μ m sieve. Then, the sieve was irrigated with Dulbecco's PBS, and the cells were collected into a 50-ml conical tube. Pelleted cells were resuspended in RP-10 and used for FACS analysis (Supplementary Figs. 2–4 and 9).

Antibody labeling cells for FACS. Homogenized cells were labeled with monoclonal antibodies for 30 min at 4°C in FACS buffer (2% FBS in Dulbecco's PBS), washed twice in FACS buffer, then fixed in 2% paraformaldehyde in Dulbecco's PBS. Panel 1 ('Adaptive' panel) included CD45 and HLA-A,B,C to discriminate TILs from other cells in the cell suspension, T cell markers CD3, CD4 and CD8, T cell activation markers OX-40 and CD127 (IL-7R α), exhaustion markers PD-1, TIM3 and LAG3 and the T cell differentiation markers CCR7 and CD45RA. Panel 2 ('T_{reg}/T cell differentiation' panel) included CD45, HLA-A,B,C, CD3, CD4, CD8, CD103, CD69, CTLA4 and FOXP3. Cells were stained via direct method (as described above for panel 1), then fixed, permeabilized and stained with the FOXP3 monoclonal antibody using the e-Bioscience fixation and permeabilization kit reagents according to the manufacturer's protocol (e-Bioscience, San Diego, CA, USA). In both panels, viable cells were revealed using the fixable viability dye (Biologics, San Diego, CA). Multiparameter FACS data was acquired on the BD LSR Fortessa X-20 FACS instrument (BD Biosciences, San Diego, CA, USA), and data was analyzed using FlowJo software (version 10, Treestar Inc., Seattle, CA, USA). A representative example of the gating strategy for panel 1 to define TILs and then T cell differentiation and activation and suppressor molecules is shown in Supplementary Fig. 2.

FACS sorting for bulk RNA-seq. TILs were isolated from three separate BC tissues, and the homogenized cells were labeled with monoclonal antibodies for 30 min at 4°C in FACS buffer (2% FBS in Dulbecco's PBS), then washed twice in FACS buffer. Viable CD3+CD8+CD69+CD103+ and CD3+CD8+CD69+CD103- T cells were sorted into Dulbecco's PBS + 0.04% BSA and retained on ice. Sorted cells were confirmed to be >85–95% pure before RNA extraction.

Breast cancer TIL functional analysis. Homogenized breast tumor cells and fresh TILs were cocultured in duplicate wells *in vitro* at 37°C for 18 h at 5 \times 10⁶ cells/ml with or without CD3/CD28 beads (Human T activator beads, Pro-Mab Catalogue no. PM-CAR2002-2ML, ProMab Biotechnologies, Richmond, CA, USA), in a TIL:bead ratio of 1:1. Golgi stop and Golgi plug (Catalog no. 554724 and 555029, BD Biosciences, San Diego, CA, USA) protein-transport inhibitors were added for 3 h before labeling with cell surface antibodies for 30 min at 4°C in FACS wash buffer. For intracellular T effector cytokine and cytotoxic granule detection, cells were fixed and permeabilized (fixation and permeabilization kit, eBioscience, catalog no. 00-5523-00, Affymetrix Inc., San Diego, CA, USA) as per the manufacturer's instructions. The monoclonal antibodies used in the FACS panel included CD45-BV510, CD3-APCH7, CD8-BV605 and CD103-BV421, IFN- γ -FITC, TNF- α -APC and GZMB-PE. Multiparameter FACS data were acquired on the BD LSR Fortessa X-20 FACS instrument (BD Biosciences, San Diego, CA). In addition, after the overnight coculture, culture supernatant was harvested and human cytometric bead array (CBA) assay performed for cytokines (IFN- γ , TNF- α , IL-2, IL-4 and GZMB) and chemokines (CCL3, CCL5) (CBA Human Immunoglobulin Flex Set System, BD Biosciences, San Diego, CA) and analyzed on a BD FACS Verse (BD Biosciences, San Diego, CA).

Single-stain immunohistochemistry. Immunohistochemistry was performed on 3- μ m serial sections of FFPE tissue using a Benchmark Ultra Autostainer (Ventana Medical Systems, Tuscon, AZ, USA). Briefly, deparaffinization and subsequent steps were done on board, including antigen retrieval with cell conditioner 1 (CC1) for 32 min at 100°C, preprimary peroxidase inhibitor for 5 min at room temperature, primary antibody incubation for 32 min at 36°C, then visualization with OptiView DAB IHC Detection Kit (Ventana Medical Systems). CD8 was detected using Novocastra liquid mouse monoclonal antibody (NCL-L-CD8-4B11, Leica Biosystems, Mt Waverley, Victoria, Australia) at a working dilution of 1:200, and CD103 was detected using Cell Marque rabbit monoclonal antibody (EP206, Cell Marque, Rocklin, CA, USA) at a working dilution of 1:100. Counterstaining was done with Mayer's Haematoxylin (Amber Scientific, Midvale, WA, Australia) for 60 s and bluing in Scott's tap water solution. Human tonsil and spleen tissues were used as controls.

Multiplex immunohistochemistry. TILs were analyzed in patient biopsy samples using the OPAL serial immunostaining protocol previously described³². The expression of CD8 and CD103 was analyzed using a similar but modified protocol described by Nolan et al.⁷ Briefly, 4- μ m FFPE sections were incubated for 30 min at room temperature with mouse anti-human CD8 (clone 4B11, 1:200, Thermo Fisher Scientific, Scoresby, Victoria, Australia) and rabbit anti-human anti-integrin alpha E (CD103) (clone EPR4166[2], 1:500, Abcam, Cambridge, MA, USA). A secondary horseradish peroxidase-conjugated antibody supplied by PerkinElmer was applied for 10 min at room temperature. Signal amplification was carried out using 100 μ l of TSA Plus working solution at a dilution of 1:100 in 1 \times amplification diluent, which was incubated at room temperature for 10 min as specified by the manufacturer (PerkinElmer, Melbourne, Victoria, Australia). Multispectral imaging was undertaken using the Vectra 3.0 (PerkinElmer) at 20 \times magnification. Image analysis, including cell segmentation, phenotyping and cell quantitation, was undertaken using the inForm Advanced Image Analysis Software (PerkinElmer) version 2.3. Between 5–10 high-power fields were taken per patient sample depending on tumor size to quantitate the average number of CD8+, CD103+ and CD8+CD103+ cells. Additionally, one stained section was imaged at 60 \times magnification using the FV3000 Confocal Laser Scanning Microscope (Olympus, Japan) to illustrate co-expression of markers.

RNA isolation and RNA sequencing. Single-cell suspensions of breast cancer tissue were obtained by enzymatic dissociation as previously described on the day of surgery, from one primary TNBC, one primary ER-negative HER2-amplified breast cancer and one TNBC liver metastasis. Viable cells were FACS-sorted on BD FACSAria II Cell Sorter (BD Biosciences) by propidium iodide staining and were further sorted for CD8+CD69+CD103+ and CD8+CD69+CD103- TIL subsets. Total RNA was extracted using the RNAqueous-4PCR RNA isolation kit (Thermo Fisher) with cell concentrations ranging between 1 \times 10⁵–2 \times 10⁵ cells for RT-PCR. Between 50 and 200 ng total RNA was used per sample. Libraries were prepared using the Illumina TruSeq RNA Sample Prep Kit v2, following the vendors protocol. Briefly, poly(A) mRNA was purified using poly(T) magnetic beads, fragmented using divalent cations under elevated temperature and reverse transcribed to cDNA with random primers. Indexed adaptors were then ligated and the libraries amplified. Fifteen to 19 cycles of PCR were necessary. Library concentration was measured using the Qubit High Sensitivity kit and fluorometer (Thermo Fisher Scientific) and the quality checked using the High Sensitivity D1000 reagents in an Agilent Tape Station. Libraries were pooled and sequenced on an Illumina NextSeq Mid Output run to generate 16–23 million 75-bp paired-end reads per sample.

Single-cell RNA sequencing. Single-cell suspensions were generated as described earlier from two individual TNBC primary tumor samples, and the viable cells were FACS-sorted for CD3+ T cells on a BD FACSAria II Cell Sorter (BD Biosciences). The cells were sorted into Dulbecco's PBS + 0.04% BSA and retained on ice. Sorted cells were then counted and assessed for viability with Trypan blue using a Countess II automated counter (Thermo Fisher Scientific). Cells were then resuspended at a 1 \times 10⁵–2 \times 10⁵ cells/ml concentration with a final viability of >80% as determined with the Countess. Single-cell library preparation was carried out as per the 10 \times Genomics Chromium single-cell protocol for the v2 reagent kit (10 \times Genomics, Pleasanton, CA, USA). Cell suspensions were loaded onto a Chromium Single-Cell Chip along with the reverse transcription (RT) master mix and single cell 3' gel beads, aiming for 2,000–6,000 cells per channel. Following generation of single-cell gel bead-in-emulsions (GEMs), reverse transcription was performed using a C1000 Touch Thermal Cycler with a Deep Well Reaction Module (Bio-Rad Laboratories, Hercules, CA, USA). Amplified cDNA was purified using SPRIselect beads (Beckman Coulter, Lane Cove, NSW, Australia) and sheared to approximately 200 bp with a Covaris S2 instrument (Covaris, Woburn, MA, USA) using the manufacturer's recommended parameters. Sequencing libraries were generated with unique sample indices (SI) for each sample. Libraries were sequenced on an Illumina HiSeq 2500 High Output Mode using V4 clustering and sequencing chemistry.

Bulk RNA-seq methods. Adaptors were trimmed from sequencing reads using Skewer (version 0.2.2)³³. Transcript quantification was performed using kallisto (version 0.43.0)³⁴, against the Ensembl transcript reference (release 79, GRCh38). Subsequent analysis was performed using R (version 3.4.0). ‘tximport’ (version 1.4.0) was used to import and aggregate transcript level data to gene level³⁵. Differential expression was performed using limma (version 3.32.8), with a design matrix encoding sample identity and the CD103+ or CD103- FACS gating as the experimental condition³⁶. Data were trimmed mean of M-values (TMM) normalized and transformed using the voom ‘WithQualityWeights’ function^{37,38}.

T cell receptor analysis. TCR-β CDR3 sequences were extracted from RNA-seq data using mixcr (version 2.1.5)^{39,40}. Adapters were trimmed from fastq files before running mixcr alignment in RNA-seq mode. Two rounds of contig assembly were performed, followed by extension of incomplete TCR CDR3 sequences. TCR-β clonotypes were exported using default settings of mixcr, which identifies clonotypes on the basis of the TCR CDR3 sequence. In bulk RNA-seq from heterogeneous tumor samples, mixcr was reported to reliably detect clonotypes with a prevalence >0.15% and has also been verified to work for RNA-seq in sorted T cell populations with a read length as low as 50 bp⁴⁰. Concordant clonotypes were determined on the basis of the CDR3 amino acid sequence. T cell clonality was calculated as 1 – (the normalized Shannon entropy of the clonotype prevalences) for a given sample²¹. Clonotype prevalence was not filtered before clonality calculation.

Single-cell RNA-seq data preprocessing. The Cell Ranger software pipeline (version 1.3.1) provided by 10xGenomics was used to demultiplex cellular barcodes, map reads to the genome and transcriptome using the STAR aligner, and down-sample reads as required to generate normalized aggregate data across samples, producing a matrix of gene counts versus cells. We processed the unique molecular identifier (UMI) count matrix using the R package Seurat (version 1.4.0.14)⁴¹. As a quality-control (QC) step, we first filtered out genes detected in less than three cells and cells where <200 genes had nonzero counts. To remove likely multiplet captures, which is a major concern in microdroplet-based experiments, we further excluded cells with total UMI counts >7,500 or the number of detected genes was >2,500. Following visual inspection of the distribution of cells by the fraction of mitochondrial genes expressed, we further discarded low-quality cells where >4% of the counts belonged to mitochondrial genes. After applying these QC criteria, 5,759 single cells and 15,623 genes in total remained and were included in downstream analyses. Library size normalization was performed in Seurat on the filtered matrix to obtain the normalized count.

Dimensionality reduction and clustering. To focus on more biologically meaningful variation, we used a subset of highly variable genes to perform unsupervised clustering. To identify highly variable genes, the *MeanVarPlot* method in the Seurat package was used to establish the mean-variance relationship of the normalized counts of each gene across cells. We then chose genes whose log-mean was between 0.015 and 3.2 and whose dispersion was above 0.5, resulting in 1,675 highly variable genes. The matrix containing raw counts for highly variable genes was further processed using ZINB-WaVE (version 0.99.4.2) to obtain the optimal low-dimensional representation of the matrix⁴². ZINB-WaVE was run with the number of latent variables set to 10, and two cell-level covariates were used: the total number of UMI counts to adjust for differences in library sizes and batch information to remove batch effects. We then performed a modularity-based clustering method with the smart local moving algorithm as implemented in the *FindClusters* function in the Seurat package on the low-dimensional representation produced by ZINB-WaVE. We set the *k.param* parameter to 25, leaving the other parameters as default. This resulted in ten distinct clusters. To visualize the clusters in two dimensions, the t-SNE map was calculated using the ZINB-WaVE output and the Rtsne package (0.13; <https://github.com/jkrijthe/Rtsne>).

Two approaches were combined to infer cell types for each cluster. First, we directly examined the expression levels of a set of canonical markers for the target cell types. Enrichment of these markers in certain clusters was considered a strong indication of the clusters representing the corresponding cell types. Because of the high dropout rate in scRNA-seq data, especially in microdroplet-based experiments, some genes suffered from a high incidence of dropout events and thus had a low signal-to-noise ratio. To remedy this, we used SAVER⁴³ (version 0.1.3) to impute predropout expression profiles. SAVER was run on the raw counts with its default setting. Enrichment of markers was then examined on the imputed data.

The second approach used genes identified to be differentially expressed as marker genes for cell-type identification. We compared gene expression in cells belonging to each cluster with that in all the other cells to obtain markers for each cluster. Here we performed differential expression (DE) analysis using the DECENT package (version 0.1.0) without spike-ins, with its default parameters⁴⁴. The DE analysis was performed using the combined data from the two samples, and we attempted to correct for possible batch effects by including a dummy batch variable in the model for the combined data. Finally, genes were ranked for evidence of DE by their *P* values (smallest to largest). The top-ranked genes are considered as markers for each cluster and can provide cell-type information.

Analysis of CD8⁺ subpopulations. To further explore features of CD8⁺ T_{RM}, we carried out a series of analyses focusing on the CD8⁺ populations (CD8⁺ T_{RM}, CD8⁺ T_{EM}, CD8⁺ γδ and CD8⁺ mitotic T_{RM}). DE analysis was performed with DECENT without spike-ins using default parameters, contrasting nonmitotic T_{RM} with non-T_{RM} cells (T_{EM} together with CD8⁺ γδ). We identified differentially expressed genes (DEGs) with absolute log fold-change > 1 and Benjamini–Hochberg adjusted *P* < 0.01. We performed a competitive gene set test using Camera⁴⁵ with the upregulated and downregulated DEGs from bulk experiment as the test gene sets. The DECENT test statistics were used as input for the preranked version of the Camera (*cameraPR* function in limma package, version 3.32.3) rank-based model.

To further confirm the cell-cycle phases of the cells, we used the Cyclone model⁴⁶ implemented in the Scran (version 1.4.5) package⁴⁷. It takes the expression levels of a set of cell-cycle related gene pairs as input to classify cells into G1, S and G2/M phase. The model was run with the preselected human gene pairs in the scran package on the raw UMI matrix.

Monocle 2 (version 2.4.0)^{14,48} was used for the trajectory analysis on the CD8⁺ populations in the first sample. Genes used for the cell ordering were determined in an unsupervised fashion by their dispersion across cells. We selected genes with mean expression ≥ 0.02 and empirical dispersion parameter estimates more than 1.5-fold greater than the fitted dispersion parameter estimates across the CD8⁺ cells. Dimensionality reduction and trajectory construction were performed on the selected genes with default methods and parameters.

Survival analyses with the tissue resident memory T cell gene signature.

In order to assess the expression and prognostic value of the T_{RM} signature (Supplementary Table 2), gene expression and survival data from the METABRIC¹⁹ dataset were accessed using CBioPortal⁵⁰ and analyzed in R. Breast cancer samples were classified by the PAM50 molecular subtype classifier⁵¹. Kaplan–Meier survival curves were generated by partitioning cases in a 25:75 split based on ranked signature expression, which was determined using the ‘sig.score’ function in the R package genefun (version 2.8.0). If fold-change values for each gene in the signature were available, this was used to weight each gene in calculating the average. For the univariable forest plots, hazard ratios were derived using Cox proportional hazards survival models using the TRM signature (genes that were significantly upregulated in the T_{RM} cluster as compared with the other clusters FDR < 1% and log fold-change > 1.0) with the endpoints of disease free and overall survival. Additional immune signatures were obtained from the literature—T follicular helper cell (T_{FH}) and T helper type 1 (T_{H1}); Teschendorff et al.²² prognostic signature (Immune 1), STAT1 signature (STAT1)²². Single gene expression of CD8A, CD3 and CD103 were also compared as a continuous variable in the Cox regression models in the METABRIC dataset. Multivariable analyses were adjusted by nodal status, tumor size, age and histological grade. All analyses were produced in R version 3.4.0.

Gene expression data for a metastatic melanoma cohort treated with checkpoint inhibitors was obtained from Riaz et al.²⁰ (data available at https://github.com/riazn/bms038_analysis/). Annotation of the patient samples and exclusion of outliers was performed as per the original study. Gene set testing between responders and nonresponders at baseline and between baseline and on-therapy biopsies for the whole cohort was performed using Camera in the R package edgeR^{45,52,53} (3.18.1), with default settings. For gene set tests accounting for both response status and baseline and on-treatment biopsies, the more flexible linear modeling framework of limma was used, estimating intersample correlation for each patient with the ‘duplicateCorrelation’ function⁵⁴. Gene set testing was performed with limma’s ‘roast’ function, with default settings⁵⁵.

Statistical analysis. All statistical analysis was performed in R (version 3.4.0). Unpaired two-sided Wilcoxon rank sum tests were used for pair-wise comparisons, and the Kruskal–Wallis rank sum test was used for comparisons between more than two groups, followed by Dunn’s test for multiple comparisons. Correlation between variables was performed using Spearman’s rank correlation, and confidence intervals were calculated according to the method of Bonett and Wright^{56,57}. Statistical significance was accepted for *P* < 0.05. For differential expression calculations in single-cell gene expression data, the DECENT package implements a likelihood ratio test to determine statistical significance⁴⁴. In bulk RNA-seq data, the R package limma fits gene-wise linear models and implements empirical Bayes moderated t-statistics to determine statistical significance³⁶. For analysis of the melanoma dataset, in addition to limma as described above, the edgeR package was used to fit gene-wise negative binomial generalized log-linear models and to determine differential expression between conditions using a log ratio test⁵³. For all differential expression and gene set testing analyses, *P* values were corrected for multiple testing using the Benjamini–Hochberg method.

Reporting summary. Further information on experimental design is available in the Nature Research Reporting Summary linked to this article.

Data availability. Raw bcl files for single-cell sequencing have been deposited at zenodo.org (<https://doi.org/10.5281/zenodo.1169607> and <https://doi.org/10.5281/zenodo.1170580>). Bam files and quantified gene counts for single-cell sequencing are available at the Gene Expression Omnibus (GEO) and Sequence Read Archive (SRA) under accession numbers GSE110686, SRX3710117 and SRX3710118. Fastq

files from bulk RNA-seq are available at the European Genome Archive under accession number EGAS00001002845 and are subject to a controlled data access agreement. Data access will be provided to any party able to comply with the associated Data Access Agreement. Bulk RNA-seq count data is available at GEO accession number GSE110938. The figures associated with the above raw datasets are Figs. 2b–f and 3a–d and Supplementary Figs. 8 and 9.

References

31. Topalian, S. L., Muul, L. M., Solomon, D. & Rosenberg, S. A. Expansion of human tumor infiltrating lymphocytes for use in immunotherapy trials. *J. Immunol. Methods* **102**, 127–141 (1987).
32. Stack, E. C., Wang, C., Roman, K. A. & Hoyt, C. C. Multiplexed immunohistochemistry, imaging, and quantitation: a review, with an assessment of Tyramide signal amplification, multispectral imaging and multiplex analysis. *Methods* **70**, 46–58 (2014).
33. Jiang, H., Lei, R., Ding, S. W. & Zhu, S. Skewer: a fast and accurate adapter trimmer for next-generation sequencing paired-end reads. *BMC Bioinformatics* **15**, 182 (2014).
34. Bray, N. L., Pimentel, H., Melsted, P. & Pachter, L. Near-optimal probabilistic RNA-seq quantification. *Nat. Biotechnol.* **34**, 525–527 (2016).
35. Soneson, C., Love, M. I. & Robinson, M. D. Differential analyses for RNA-seq: transcript-level estimates improve gene-level inferences. *F1000Res* **4**, 1521 (2015).
36. Ritchie, M. E. et al. limma powers differential expression analyses for RNA-sequencing and microarray studies. *Nucleic Acids Res.* **43**, e47 (2015).
37. Law, C. W., Chen, Y., Shi, W. & Smyth, G. K. voom: Precision weights unlock linear model analysis tools for RNA-seq read counts. *Genome Biol.* **15**, R29 (2014).
38. Liu, R. et al. Why weight? Modelling sample and observational level variability improves power in RNA-seq analyses. *Nucleic Acids Res.* **43**, e97 (2015).
39. Bolotin, D. A. et al. MiXCR: software for comprehensive adaptive immunity profiling. *Nat. Methods* **12**, 380–381 (2015).
40. Bolotin, D. A. et al. Antigen receptor repertoire profiling from RNA-seq data. *Nat. Biotechnol.* **35**, 908–911 (2017).
41. Macosko, E. Z. et al. Highly parallel genome-wide expression profiling of individual cells using nanoliter droplets. *Cell* **161**, 1202–1214 (2015).
42. Risso, D., Perraudeau, F., Gribkova, S., Dudoit, S. & Vert, J.-P. ZINB-WaVE: a general and flexible method for signal extraction from single-cell RNA-seq data. *Preprint at* <https://doi.org/10.1101/125112> (2017).
43. Huang, M. et al. SAVER: Gene expression recovery for UMI-based single cell RNA sequencing. *Preprint at* <https://doi.org/10.1101/138677> (2017).
44. Ye, C., Speed, T. P. & Salim, A. DECENT: differential expression with capture efficiency adjustment for single-cell RNA-seq data. *Preprint at* <https://doi.org/10.1101/225177> (2017).
45. Wu, D. & Smyth, G. K. Camera: a competitive gene set test accounting for inter-gene correlation. *Nucleic Acids Res.* **40**, e133 (2012).
46. Scialdone, A. et al. Computational assignment of cell-cycle stage from single-cell transcriptome data. *Methods* **85**, 54–61 (2015).
47. Lun, A. T., McCarthy, D. J. & Marioni, J. C. A step-by-step workflow for low-level analysis of single-cell RNA-seq data with Bioconductor. *F1000Res* **5**, 2122 (2016).
48. Qiu, X. et al. Reversed graph embedding resolves complex single-cell trajectories. *Nat. Methods* **14**, 979–982 (2017).
49. Curtis, C. et al. The genomic and transcriptomic architecture of 2,000 breast tumours reveals novel subgroups. *Nature* **486**, 346–352 (2012).
50. Gao, J. et al. Integrative analysis of complex cancer genomics and clinical profiles using the cBioPortal. *Sci. Signal.* **6**, pl1 (2013).
51. Perou, C. M. et al. Molecular portraits of human breast tumours. *Nature* **406**, 747–752 (2000).
52. McCarthy, D. J., Chen, Y. & Smyth, G. K. Differential expression analysis of multifactor RNA-Seq experiments with respect to biological variation. *Nucleic Acids Res.* **40**, 4288–4297 (2012).
53. Robinson, M. D., McCarthy, D. J. & Smyth, G. K. edgeR: a Bioconductor package for differential expression analysis of digital gene expression data. *Bioinformatics* **26**, 139–140 (2010).
54. Smyth, G. K., Michaud, J. & Scott, H. S. Use of within-array replicate spots for assessing differential expression in microarray experiments. *Bioinformatics* **21**, 2067–2075 (2005).
55. Wu, D. et al. ROAST: rotation gene set tests for complex microarray experiments. *Bioinformatics* **26**, 2176–2182 (2010).
56. Bonett, D. G. & Wright, T. A. Sample size requirements for estimating pearson, kendall and spearman correlations. *Psychometrika* **65**, 23–28 (2000).
57. Bishara, A. J. & Hittner, J. B. Confidence intervals for correlations when data are not normal. *Behav. Res. Methods* **49**, 294–309 (2017).

Reporting Summary

Nature Research wishes to improve the reproducibility of the work that we publish. This form provides structure for consistency and transparency in reporting. For further information on Nature Research policies, see [Authors & Referees](#) and the [Editorial Policy Checklist](#).

Statistical parameters

When statistical analyses are reported, confirm that the following items are present in the relevant location (e.g. figure legend, table legend, main text, or Methods section).

n/a Confirmed

- The exact sample size (n) for each experimental group/condition, given as a discrete number and unit of measurement
- An indication of whether measurements were taken from distinct samples or whether the same sample was measured repeatedly
- The statistical test(s) used AND whether they are one- or two-sided
 - Only common tests should be described solely by name; describe more complex techniques in the Methods section.*
- A description of all covariates tested
- A description of any assumptions or corrections, such as tests of normality and adjustment for multiple comparisons
- A full description of the statistics including central tendency (e.g. means) or other basic estimates (e.g. regression coefficient) AND variation (e.g. standard deviation) or associated estimates of uncertainty (e.g. confidence intervals)
- For null hypothesis testing, the test statistic (e.g. F , t , r) with confidence intervals, effect sizes, degrees of freedom and P value noted
 - Give P values as exact values whenever suitable.*
- For Bayesian analysis, information on the choice of priors and Markov chain Monte Carlo settings
- For hierarchical and complex designs, identification of the appropriate level for tests and full reporting of outcomes
- Estimates of effect sizes (e.g. Cohen's d , Pearson's r), indicating how they were calculated
- Clearly defined error bars
 - State explicitly what error bars represent (e.g. SD, SE, CI)*

Our web collection on [statistics for biologists](#) may be useful.

Software and code

Policy information about [availability of computer code](#)

| | |
|-----------------|---|
| Data collection | Multiplex immunohistochemistry imaged using the commercial software inForm Advanced Image Analysis Software (PerkinElmer) version 2.3 |
| Data analysis | General data analysis, include statistical tests, data compilation and plotting: R 3.4.0 with the packages ggplot2 (2.2.1), dplyr (0.7.4), plyr (1.8.4), tidyr (0.7.1), readr (1.1.1), dunn.test(1.3.4), ggrepel (0.7.0), ggsignif (0.4.0), broom (0.4.2), readxl (1.0.0), survival (2.41-3), genefu (2.10.0). FACS data analysis: FlowJo v10 software (Treestar Inc. Seattle, CA, USA). Single Cell Data analysis: Cellranger pipeline (10X Genomics, version 1.3.1). Subsequent analysis in R using the packages Seurat (1.4.0.14), scran (1.4.5), SAVER (0.1.3) zinbwave (0.99.4.2), Rsne (0.13), Monocle 2 (2.4.0). Differential expression analysis was performed using DECENT, which is described in detail in this openly available preprint, which also contains details of software availability (https://www.biorxiv.org/content/early/2017/11/26/225177). The DECENT source code is hosted at https://github.com/cz-ye/DECENT Bulk RNASeq: Alignment and transcript quantification with kallisto (0.43.0). Subsequent analysis in R using tximport (1.4.0), limma (3.32.8), edgeR (3.18.1), ensemblldb (2.0.4), EnsDb.Hsapiens.v79 (2.1.0) and the packages previously described. TCR analysis was performed using mixcr (2.1.5). Normalized Shannon entropy was calculated using the R package vegan (2.4-6). Web application uses the R package shiny (1.0.5) and plotly (4.7.1). |

For manuscripts utilizing custom algorithms or software that are central to the research but not yet described in published literature, software must be made available to editors/reviewers upon request. We strongly encourage code deposition in a community repository (e.g. GitHub). See the Nature Research [guidelines for submitting code & software](#) for further information.

Data

Policy information about [availability of data](#)

All manuscripts must include a [data availability statement](#). This statement should provide the following information, where applicable:

- Accession codes, unique identifiers, or web links for publicly available datasets
- A list of figures that have associated raw data
- A description of any restrictions on data availability

Raw bcl files for single cell sequencing have been deposited at zenodo.org (10.5281/zenodo.1169607 and 10.5281/zenodo.1170580). Bam files and quantified gene counts for single cell sequencing are available at GEO and SRA, accessions GSE110686, SRX3710117 and SRX3710118. Fastq files from bulk RNASeq are available at the European Genome Archive, accession number EGAS00001002845 and are subject to a controlled data access agreement. Data access will be provided to any party able to comply with the associated Data Access Agreement. Bulk RNASeq count data is available at GEO accession number GSE110938. Figures associated with the above raw datasets: Figs. 2b-f; Figs. 3a-c and 3d; Supplementary Figs 8 and 9.

Field-specific reporting

Please select the best fit for your research. If you are not sure, read the appropriate sections before making your selection.

Life sciences Behavioural & social sciences Ecological, evolutionary & environmental sciences

For a reference copy of the document with all sections, see nature.com/authors/policies/ReportingSummary-flat.pdf

Life sciences study design

All studies must disclose on these points even when the disclosure is negative.

| | |
|-----------------|---|
| Sample size | In an exploratory study of this nature it is not possible to pre-specify the sample size. Cases were acquired and data analyzed prospectively. The final sample size was determined in an adaptive fashion, based on the degree of variability seen between cases and the need to equally represent tumours from each breast cancer subtype across primary and metastatic samples. |
| Data exclusions | The CONSORT diagram (Supplementary figure 1) and demographics table (Supplementary Table 1) describe the sample selection and exclusion. Some samples were excluded due to technical failure, for example, the inability to acquire any FACS data. No samples were excluded after successful analysis. For the functional studies presented in Figure 4e, not all cytokines assayed were presented, as they exist on the panel are not relevant to the paper. |
| Replication | All characterisations of tumor infiltrating lymphocytes by flow cytometry, immunohistochemistry, and functional assays were replicated at least 5 times on different patient's samples. Single cell sequencing was performed on 2 independent cases. Bulk RNASeq was performed on 3 independent cases. |
| Randomization | As no therapeutic interventions were undertaken, randomization is not relevant. |
| Blinding | The methods employed in this study involve unbiased quantification by flow cytometry, immunohistochemistry or gene expression. There was no therapeutic intervention or expected outcome prior to performing these analysis, therefore blinding is not relevant. |

Reporting for specific materials, systems and methods

Materials & experimental systems

| | |
|-------------------------------------|---|
| n/a | Involved in the study |
| <input type="checkbox"/> | <input checked="" type="checkbox"/> Unique biological materials |
| <input type="checkbox"/> | <input checked="" type="checkbox"/> Antibodies |
| <input checked="" type="checkbox"/> | <input type="checkbox"/> Eukaryotic cell lines |
| <input checked="" type="checkbox"/> | <input type="checkbox"/> Palaeontology |
| <input checked="" type="checkbox"/> | <input type="checkbox"/> Animals and other organisms |
| <input type="checkbox"/> | <input checked="" type="checkbox"/> Human research participants |

Methods

| | |
|-------------------------------------|--|
| n/a | Involved in the study |
| <input checked="" type="checkbox"/> | <input type="checkbox"/> ChIP-seq |
| <input type="checkbox"/> | <input checked="" type="checkbox"/> Flow cytometry |
| <input checked="" type="checkbox"/> | <input type="checkbox"/> MRI-based neuroimaging |

Unique biological materials

Policy information about [availability of materials](#)

Obtaining unique materials

The unique materials in this study constitute patient samples. Fresh samples are in general not available, usually having been consumed for the analyses presented.

Antibodies

Antibodies used

Listed as - Antibody: supplier, clone name, lot number, fluorochrome (for FACS), catalogue number.

Multiplex IHC:

PD-1: Bio SB, EP239, 3153BHC23, BSB3152.
 CD3: Spring Bioscience, SP7, 150407LVS, M3072/06970311001.
 CD8: ThermoFisher, 4B11, SA2321871, MA1-80231.
 CD103: Abcam, EPR4166[2], GR223668-19, Ab129202.

Flow cytometry antibodies:

GZMB: BD Biosciences, GB11, 7026751, 561142, PE.
 FoxP3: eBioscience, PCH101, E09963-1635, 12-4776-42, PE.
 CD8a: BD Biosciences, HIT8a, 6095935, 555635, PE.
 CD8a: Biolegend, RPA-T8, B230656, 301040, BV605.
 HLA ABC: BD Biosciences, G46-2.6, 5163888, 555554, PE-Cy5.
 CD69: Biolegend, FN50, B210943, 310912, PE-Cy7.
 CD69: Biolegend, FN50, B234158, 310926, PerCP-Cy5.5.
 CD152,CTLA-4: Biolegend, L3D10, B185662, 349908, APC.
 CD223,LAG3: RD Systems, 874501, ADXMO114071, FAB23193A, APC.
 CD3e: BD Biosciences, SK7, 7234624, 560176, APC-H7.
 CD3: BD Biosciences, SK7, 7040875, 564560, BB515 (FITC).
 CD127,IL-7Ra: Biolegend, A019D5, B205137, 351310, BV421.
 CD103,ITGAE: Biolegend, BerACT8, B238177, 350214, BV421.
 CD45: Biolegend, H130, B2411217, 304036, BV510.
 CD4: Biolegend, OKT4, B2300991, 317436, BV650.
 CD4: Biolegend, SK3, 7186973, 340443, APC.
 CD197,CCR7: Biolegend, G043H7, B223097, 353228, BV711.
 CD279,PD-1: Biolegend, EH12.2H7, B2362550, 329930, BV785.
 CD134,OX40: Biolegend, Ber-ACT35, B2034472, 350012, PE-Cy7.
 CD366,TIM3: eBioscience, F38-2E2, 4272530, 46-3109-42, PerCP-eFlor710.
 CD45RA: BD Biosciences, HI100, 5181589, 555488, FITC.
 CD45: BD Biosciences, H130, 4248832, 555482, FITC.

Validation

Multiplex IHC:

PD-1: Bio SB, EP239 - Validated on human peripheral blood lymphocytes as per manufacturer.
 CD3: Spring Bioscience, SP7 - Validated against human lymphoid tissues as per manufacturer.
 CD8: ThermoFisher, 4B11 - Validated in human tissues as per manufacturer.
 CD103: Abcam, EPR4166[2] - Validated in human T-cell populations in multiple publications (Wang et al, 2016 CCR 22(24)6290-97; Stelma et al, 2017 Sci Rep 7(1):6172).

Flow cytometry antibodies:

GZMB: BD Biosciences, GB11 - Validated on human peripheral blood lymphocytes as per manufacturer.
 FoxP3: eBioscience, PCH101 - Validated on human peripheral blood lymphocytes as per manufacturer.
 CD8a: BD Biosciences, HIT8a - Validated on human peripheral blood lymphocytes as per manufacturer.
 CD8a: Biolegend, RPA-T8 - Validated on human peripheral blood lymphocytes as per manufacturer.
 HLA ABC: BD Biosciences, G46-2.6 Validated on human peripheral blood lymphocytes as per manufacturer.
 CD69: Biolegend, FN50 - Validated on PMA+ionomycin activated human peripheral blood lymphocytes as per manufacturer.
 CD152,CTLA-4: Biolegend, L3D10 - Validated on human peripheral blood lymphocytes as per manufacturer.
 CD223,LAG3: RD Systems, 874501 - Validated on human peripheral blood lymphocytes as per manufacturer.
 CD3e: BD Biosciences, SK7 - Validated on human peripheral blood lymphocytes as per manufacturer.
 CD3: BD Biosciences, SK7 - Validated on human peripheral blood lymphocytes as per manufacturer.
 CD127,IL-7Ra: Biolegend, A019D5 - Validated on human peripheral blood lymphocytes as per manufacturer.
 CD103,ITGAE: Biolegend, BerACT8 - Validated on PHA-stimulated human peripheral blood lymphocytes as per manufacturer.
 CD45: Biolegend, H130 - Validated on human peripheral blood lymphocytes as per manufacturer.
 CD4: Biolegend, OKT4 - Validated on human peripheral blood lymphocytes as per manufacturer.
 CD4: Biolegend, SK3 - Validated on human peripheral blood lymphocytes as per manufacturer.
 CD197,CCR7: Biolegend, G043H7 - Validated on human peripheral blood lymphocytes as per manufacturer.
 CD279,PD-1: Biolegend, EH12.2H7 - Validated on human peripheral blood lymphocytes as per manufacturer.
 CD134,OX40: Biolegend, Ber-ACT35 - Validated on PHAstimulated human peripheral blood lymphocytes as per manufacturer.
 CD366,TIM3: eBioscience, F38-2E2 - Validated on human peripheral blood lymphocytes as per manufacturer.
 CD45RA: BD Biosciences, HI100 - Validated on human peripheral blood lymphocytes as per manufacturer.
 CD45: BD Biosciences, H130 - Validated on human peripheral blood lymphocytes as per manufacturer.

Human research participants

Policy information about [studies involving human research participants](#)

Population characteristics

Total patients with data n = 123
 Total samples with data n = 129
 Primary tumours n = 84 (65%)
 Lymph node metastases n = 19 (19%)
 Other metastases n = 26 (20%)

Primary tumours
 Stage 1 - 3: n = 67
 Stage 4: n = 17
 Mean age: 52.5 (min 27 - max 85)
 Mean tumour size: 37.2 mm (min 12mm - max 145mm)
 Nodal status: Positive 36 (57%), Negative 27 (43%)

Metastatic tumours
 Mean age: 53.4 (min 40 - max 73)

Recruitment

Patient with primary or metastatic breast cancer were invited to participate by clinicians. There was no self-referral. Primary tumours are required to be above a certain size (usually 15mm) for tissue collection to be feasible alongside diagnostic requirements.

Flow Cytometry

Plots

Confirm that:

- The axis labels state the marker and fluorochrome used (e.g. CD4-FITC).
- The axis scales are clearly visible. Include numbers along axes only for bottom left plot of group (a 'group' is an analysis of identical markers).
- All plots are contour plots with outliers or pseudocolor plots.
- A numerical value for number of cells or percentage (with statistics) is provided.

Methodology

Sample preparation

Isolation of TILs from Breast Cancer Biopsies and normal breast tissue.

Following tumor excision, a representative tumor fragment was transferred fresh and sterile to the laboratory for study. All surrounding macroscopic tissue was removed from the tumor including any obvious tumor capsule. Tumor tissue was divided into segments and either placed in neutral buffered formalin for processing to formalin fixed paraffin embedded blocks, or a single cell suspension was created from the breast biopsy using a modified published protocol. Briefly, tumor was initially divided into segments and then finely diced into RPMI1640 containing 20% foetal bovine serum, 1mg/ml collagenase type 4 (Worthington biochemical, Lakewood, NJ), 30U/ml DNase (Roche diagnostics, Indianapolis, IN), 10ug/ml gentamicin (Life Technologies, Waltham, MA) and incubated for 30 minutes at 37°C on a rocker. Digested tumor pieces were teased thru a 70um sieve, the sieve irrigated with DPBS and the cells collected into a 50 ml conical tube. Pelleted cells were resuspended in RP-10 and used for FACS analysis.

Instrument

BD Fortessa X-20

Software

BD FACSDIVA acquisition software (BD Biosciences)
 Flowjo v10 analysis software (Treestar Inc. Seattle, CA, USA)

Cell population abundance

The purity of flow sorted CD8+CD103+CD69+ and CD8+CD103-CD69+ populations for bulk RNASeq was confirmed by returning sorted fractions to the flow cytometer, which confirmed that the target population constituted > 85% of the sorted cells. This was performed on three separate patients for RNA seq analysis.
 In addition, flow sorting was performed to derive viable CD45+CD3+ cells from 2 primary tumours for single cell mRNASeq. In this workflow, the viability of sorted cells was checked with an automated cell counter, the Countess II (Thermo Fisher Scientific), and found to be 65% and 66% for two cases. Furthermore, analysis of single cell gene expression profiles passing quality control showed a highly pure population, with only 28/5759 cells lacking CD3 expression, suggesting a purity of 99.5%.

Gating strategy

Gating strategy used to derive collated data in Figure 1 and Supplementary Fig 5 (see Supplementary Fig 2) . Viable cells were gated for MHC class I+CD45+ cells (TILs), T cells (CD3+) and CD3+CD4+ or CD3+CD8+ cells, and the % cells expressing PD-1, TIM-3, OX-40 or CD127 assessed. In addition, T cell differentiation status (naïve, central or effector memory) was assessed using CD45RA and CCR7.
 Gating strategy used to derive collated data in Figure 1c-d (see Supplementary Fig 3). Viable cells were gated for MHC class I+CD45+ cells (TILs), T cells (CD3+) and CD3+CD4+ or CD3+CD8+ cells, T cell differentiation status (naïve, central or effector memory) was assessed using CD45RA and CCR7. In addition, the % CD3+CD4+ CD103+ or CD3+CD8+CD103+ cells which express

PD-1 was also assessed.

Gating strategy was used to derive collated data in Supplementary Fig 7 and Supplementary Fig 10c (see Supplementary Fig 4). Viable cells were gated for MHC class I+CD45+ cells (TILs), T cells (CD3+) and CD3+CD4+ or CD3+CD8+ cells in (A) and the T cell differentiation status (naive, central or effector memory) assessed using CD45RA and CCR7, followed by correlation between the % T cells which expressed PD-1, CD103 or CTLA-4. In (B) the % CD3+CD4+ CD103+ or CD3+CD8+CD103+ cells which expressed PD-1, CTLA-4 or FoxP3 was also assessed.

Gating strategy for Fig 3D. Viable cells were gated for CD45+CD3+, CD3+CD8+CD103+ or CD3+CD8+CD103-and intracellular granzyme B expression assessed.

For all FACS analyses described above, positive vs negative expression was based on isotype and FMO controls.

Gating strategy for Supplementary Fig 12 (see Supplementary Fig 13). Viable cells were gated for MHC class I+CD45+ cells, T cells (CD3+) and CD3+CD4+ or CD3+CD8+ cells, and the % cells expressing CD103 and CD69 (TRMs).

Tick this box to confirm that a figure exemplifying the gating strategy is provided in the Supplementary Information.